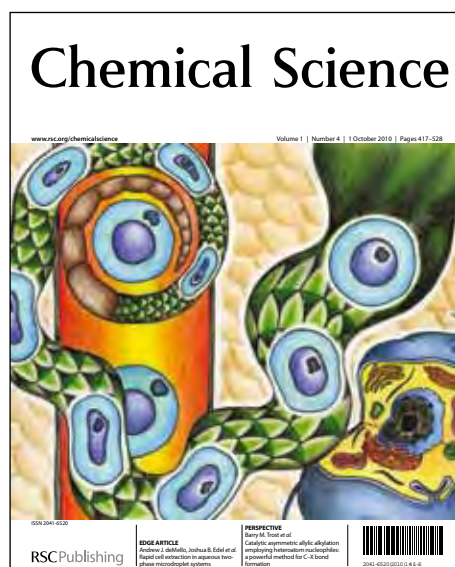


Chemical Science

Accepted Manuscript

This article can be cited before page numbers have been issued, to do this please use: M. Gruden-Pavlovic, M. Peric, P. Garcia Fernandez and M. Zlatar, *Chem. Sci.*, 2013, DOI: 10.1039/C3SC52984C.



This is an *Accepted Manuscript*, which has been through the RSC Publishing peer review process and has been accepted for publication.

Accepted Manuscripts are published online shortly after acceptance, which is prior to technical editing, formatting and proof reading. This free service from RSC Publishing allows authors to make their results available to the community, in citable form, before publication of the edited article. This *Accepted Manuscript* will be replaced by the edited and formatted *Advance Article* as soon as this is available.

To cite this manuscript please use its permanent Digital Object Identifier (DOI®), which is identical for all formats of publication.

More information about *Accepted Manuscripts* can be found in the [Information for Authors](#).

Please note that technical editing may introduce minor changes to the text and/or graphics contained in the manuscript submitted by the author(s) which may alter content, and that the standard [Terms & Conditions](#) and the [ethical guidelines](#) that apply to the journal are still applicable. In no event shall the RSC be held responsible for any errors or omissions in these *Accepted Manuscript* manuscripts or any consequences arising from the use of any information contained in them.

Theoretical study of the magnetic anisotropy and magnetic tunneling in mononuclear Ni(II) complexes with potential molecular magnet behavior[†]

Maja Gruden-Pavlović,^a Marko Perić,^b Matija Zlatar,^b and Pablo García-Fernández^{*c}

Received Xth XXXXXXXXXXXX 20XX, Accepted Xth XXXXXXXXXXXX 20XX

First published on the web Xth XXXXXXXXXXXX 200X

DOI: 10.1039/b000000x

Magnetic molecules that present a slow decay of their magnetization (molecular magnets) are very interesting both from a fundamental and applied points of view. While many approaches focus strongly in finding systems with strong magnetic anisotropy giving rise to large spin-reversal barriers, less is known on the behavior of magnetic tunneling, which is a also fundamental component of molecular magnet behavior. In this work we propose a model to describe both the spin-reversal barrier and magnetic tunneling in Ni(II) trigonal bipyramidal complexes, that could be easily extended to other transition-metal systems. Based on this model we show the criteria that lead to optimal complexes to find molecular magnet behavior. We test our proposal with multi-reference configuration-interaction (MRCI) and ligand-field-density-functional-theory (LF-DFT) first-principles calculations applied over several families of mononuclear Ni(II) complexes. As a salient result we find that the complex $[\text{NiCl}_3(\text{Hdabco})_2]^+$ (dabco is 1,4-diazabicyclo[2.2.2]-octane) displays both a very large magnetic anisotropy energy, 524 cm^{-1} , and a small tunneling splitting, 0.2 cm^{-1} , when compared to other systems containing the same metal, making it a very attractive potential molecular magnet. These values are reached due to the choice of ligands that favor a complete destruction of the Jahn-Teller distortions through the spin-orbit coupling and an unquenched orbital momentum.

1 Introduction

The creation of molecular-size devices displaying two (or more) states with distinguishable properties (i.e. *spin-up/spin-down*) at room temperature, and which are switchable under an external perturbation will pave the way towards a myriad applications in fields like high-density information storage^{1,2}, quantum-computation³ or molecular spintronics⁴. While several classes of these *bistable* systems exist^{5,6}, single molecule magnets^{1,7–11} (SMM) where each state represents a different magnetization that relaxes very slowly are, perhaps, the ones that have attracted highest expectations for practical application.

In the literature⁷ the slow relaxation present in SMMs is related to the existence of a high spin-reversal barrier, U_{eff} , that separates the states with positive and negative values of the

magnetic moments, M_s , with respect to the axis of magnetization (z). In other words, magnetic anisotropy manifests itself through an energy barrier that must be overcome to switch the magnetization from parallel to anti-parallel alignment. In axial systems, this barrier is determined by the spin-Hamiltonian:

$$\hat{H} = D\hat{S}_z^2 \quad (1)$$

where D is the axial Zero-Field-Splitting (ZFS) parameter, and \hat{S}_z^2 the projection operator of the total spin along the z -axis. From Eq. 1 we see that when D is negative, the spin-reversal barrier is $U_{\text{eff}} = |D|M_{\text{max}}^2$, where M_{max} is maximum projection of the magnetic moment of the system along z axis. While this solution seems to indicate that the optimal strategy to enhance the barrier in SMMs is increasing M_{max} by, for example, creation of polynuclear coordination clusters¹² with large magnetic moment, experimental results^{13–16} supported by theoretical modeling^{17,18} indicate that the nature of the magnetic anisotropy is local^{19,20} and that any increase in M_{max} is usually compensated by a corresponding decrease in $|D|$.

New approaches have arose to circumvent this difficulty like, for example, the use of molecules containing a single magnetic rare-earth complex^{10,11,13,21–24} where the high spin-orbit coupling of the lanthanide/actinide ion provides the system with a large magnetic anisotropy and SMM behavior. This interest in single-ion-magnets (SIM) has been lately been re-

[†] Electronic Supplementary Information (ESI) available: Vibronic theory, LF-DFT procedure and all non-empirically determined LF parameters, Detailed LF-DFT results, Structural results on GGA and LDA level, Cartesian coordinates of all the studied complexes optimized at B3LYP level. See DOI: 10.1039/b000000x/

^a Faculty of Chemistry, University of Belgrade, Belgrade, Serbia.

^b Center for Chemistry, Institute of Chemistry, Technology and Metallurgy, University of Belgrade, Njegoševa 12, P.O. Box 815, 11001 Belgrade, Serbia.

^c Departamento de Ciencias de la Tierra y Física de la Materia Condensada, Universidad de Cantabria, Avenida de los Castros s/n, 39005 Santander, Spain. E-mail: garciapa@uican.es

inforced due to the recent discovery of transition-metal complexes^{15,18,25–31} belonging to this family. In these cases the moderate spin-orbit coupling can be put to good use if symmetry considerations allows it to act at first order. Typical examples involve Co(II) or Fe(II)^{15,25,30,31} complexes but other examples, like the recent discovery of a Fe(I) complex with the highest U_{eff} found so far in a transition-metal SIM (226 cm^{-1}) are also known. Moreover, theoretical predictions have worked out many other possibilities that could lead to large, negative D values and, possibly, SIM behavior³².

From the perspective of this work, Ni(II) trigonal-bipyramidal (TBP) complexes are very interesting. While, so far, no Ni(II) SIM has been discovered, a recent theoretical-experimental work²⁹ shows that complexes of this kind can display large magnetic anisotropies with $|D|$ values of 120–180 cm^{-1} . The factors making this value much smaller than the spin-orbit constant of the isolated Ni(II) ion ($\zeta = 675 \text{ cm}^{-1}$ according to Ref.³³) is theoretically well understood²⁹. Both covalency with the ligands, and the partial quenching of the spin-orbit coupling due to its competition with the Jahn-Teller (JT) distortions reduce $|D|$ from its ideal, ionic value. However, the understanding of other magnitudes, like the *rhom-bic* ZFS splitting constant, E , is much less developed. This is somewhat surprising, as this parameter controls (in integer spin systems) the magnetic tunneling splitting³⁴ and blocking temperature, both quantities being crucial to know whether a high- $|D|$ transition metal complex will be a SIM and up to which temperature. Since these properties essentially determine whether any of these interesting molecules could find application in real-life problems we have developed a simple model to describe it and find the main chemical factors influencing its value (see Section 2). The relatively simple nature of the ground state of Ni(II)-TBP complexes (from the point of view of the number of states involved to create a realistic theory) and the interest in finding a SIM containing this ion makes these systems an ideal starting place to develop this model. In Section 4 we test the model against *ab initio* calculations and show that $[\text{NiCl}_3(\text{Xdabco})_2]^+$ (dabco is 1,4-diazabicyclo[2.2.2]-octane) ions, existing in crystal form,^{35,36} not only display a huge magnetic anisotropy with $U_{\text{eff}} = 524 \text{ cm}^{-1}$ but also present a tunneling rate which is, at least, an order of magnitude smaller than the interesting complexes recently reported by Ruamps et al.²⁹. Even though no Ni(II) SIM has been found, the properties of this complex make it susceptible to sustain a magnetization over time under the influence of a small magnetic field. If experimentally confirmed this complex would be the first of its kind.

2 Theory

In this section we will study the conditions leading to large magnetic anisotropy in Ni(II) trigonal-bipyramidal com-

plexes, and the factors determining the stability of the spin states in them. In particular, we will focus on the case where the transition metal ion is coordinated to three equivalent ligands in the plane and axial ligands differ from them. From the theoretical point of view this gives rise to two main cases³⁷ belonging to different point groups. We will initially focus on D_{3h} complexes with a horizontal symmetry plane, and will consider at a later step the effects of lowering the symmetry to D_3 , C_{3v} or C_3 .

We will start describing the electronic structure of TBP Ni(II) complexes. A basic orbital scheme is shown in Fig. 1 where $Ni(3d)$ levels are populated with 8 electrons. These complexes can be high ($S=1$) or low ($S=0$) spin, depending on the strength of ligands which control the separation of the $a'_1(d_{z^2})$ orbital from the $e'(d_{x^2-y^2}, d_{xy})$ one. We will exclusively focus on the high-spin complexes that appear with ligands like Cl or F, since the low-spin ones are not magnetic. In the former case, the ground state term is ${}^3E'$ (see Fig. 1). While the high-magnetic anisotropy of TBP-Ni(II) systems is essentially a consequence of the degenerate nature of the ground state (see for example²⁹) other properties, like magnetic tunneling, can only be recovered when excited states are considered. In all the Ni(II) complexes that we have studied using *ab initio* calculations (see Section 4) there is a group of low-lying excited states (usually within 0.7 eV) separated from the rest (usually present at energies higher than 1 eV). Our first-principles calculations indicate that many features of the spin-stability can be understood taking into account these lower states, and neglecting the effect of the higher ones.

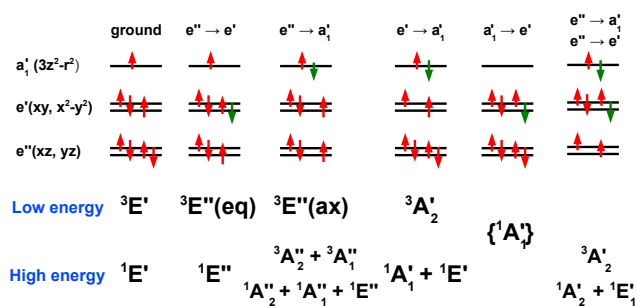


Fig. 1 (Color online) In the upper part the electronic configurations associated to a D_{3h} TBP d^8 configuration are shown, as well as the excitations from the $S = 1$ ground state. In the lower part we show the excited states spanned by each configuration classified in low and high-lying excited states. Magnetic properties are most influenced by the lower excited states. The braces around the ${}^1A'_1$ state indicate that this state can be at low (ground) or high energy depending on the ligand field strength.

2.1 The Jahn-Teller effect in TBP complexes

As indicated above the ground state of these systems is ${}^3E'$, which contains six multiplets, due to both orbital and spin degeneracy. As it is well known, orbitally degenerate systems are subject to the Jahn-Teller effect that favors a symmetry-lowering distortion of the system.³⁸ As a consequence of this motion, the degenerate levels split and the system becomes more stable.

In the case of TBP complexes, symmetry considerations indicate that only e' vibrations can vibronically couple to the ground ${}^3E'$ state. For a basic NiX_5 D_{3h} complex there are 3 normal modes that belong to this irrep. Internal coordinates that describe the distortions of a TBP molecule, are depicted in Fig. 2. It is noteworthy to point out that, while all the modes reduce symmetry to C_{2v} , the problem is still more complex than, for example the $E \otimes e$ one in octahedral systems where a single mode is JT active. For Ni(II) TBP complexes, as the degenerate orbitals ($d_{x^2-y^2}$ and d_{xy}), expand over the equatorial plane, the most important distortion is described by the angle α controlling the distortion of the equilateral triangle formed by equatorial ligands into an obtuse or acute one. The second motion in importance is given by β , the bending of the axial ligands. These two distortions chemically portray the transformation of the TBP complex into a square pyramidal one, following a Berry pseudorotation³⁹. It is important to note that the distortions described by α and β are strongly coupled. While in most simple triangular molecules the distortion that makes α smaller than 120° is favored due to anharmonic ligand-ligand interactions⁴⁰, in TBP systems this motion allows the axial ligands to relax into the plane favoring β to be smaller than 180° , which in turn pushes the equatorial ligands toward smaller α values. As we will see in Section 4, this mechanism can be used to reduce the global JT distortion, and enhance the complex magnetic anisotropy by choosing bulky ligands that cannot fit in between the equatorial ligands.

As vibronic coupling interactions conserve spin³⁸, the JT effect in the six-state ${}^3E'_\alpha$ (s_z is the spin projection and $\alpha = x^2 - y^2, xy$ the occupied e' orbital) problem can be reduced to 3 equivalent 2-by-2 $E \otimes e$ matrices. In order to take into account the spin-orbit coupling in the next step it is better to use Longuet-Higgins's complex-valued wavefunctions^{37,41}:

$$|{}^3_{s_z}E'_+\rangle = \frac{1}{\sqrt{2}} \left(|{}^3_{s_z}E_{x^2-y^2}\rangle + i |{}^3_{s_z}E_{xy}\rangle \right) \quad (2)$$

$$|{}^3_{s_z}E'_-\rangle = \frac{1}{\sqrt{2}} \left(|{}^3_{s_z}E_{x^2-y^2}\rangle - i |{}^3_{s_z}E_{xy}\rangle \right) \quad (3)$$

as the resulting states, when only considering metal orbitals, have well-defined, unquenched orbital angular momentum ($E'_\pm \rightarrow L = \pm 2$). Defining the complex vibrational modes $Q_\pm = Q_x \pm iQ_y$, where Q_x and Q_y are the two components of

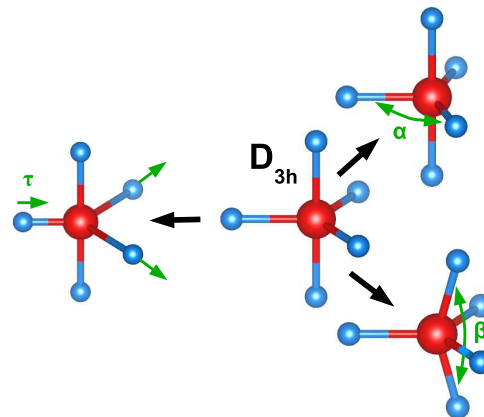


Fig. 2 (Color online) Scheme representing the three Jahn-Teller distortions for a simple NiX_5 TBP complex and the internal coordinates α , β and τ that are employed to describe them.

an e' mode and using Eqs. 2 and 3 we can obtain the linear JT coupling matrix for each spin as:

$$H_{JT}(s_z) = \frac{1}{2}K (|Q_+|^2 + |Q_-|^2) + \begin{pmatrix} 0 & -v_{E'}Q_+ \\ -v_{E'}Q_- & 0 \end{pmatrix} \quad (4)$$

where K is the force constant of the system along the mode Q and $v_{E'}$ is the linear JT constant for the ground E' state. Diagonalization of the above matrix yields a splitting of the orbital states which is linear with $\rho = \sqrt{Q_+^2 + Q_-^2}$ but these solutions retain a triple degeneracy due to the spin. Before obtaining these analytical solutions, we will first introduce the effect of the spin-orbit coupling.

2.2 Spin-orbit coupling in the ${}^3E'$ term

The spin-orbit operator in D_{3h} symmetry spans the $a'_2(l_z)$ and $e''(l_x, l_y)$ irreps. This means that only the component transforming like a'_2 can couple the states within the ${}^3E'$ term. As this operator conserves the projection of the spin (s_z) the results can still be represented by 2-by-2 matrices as we employed in the previous section. In particular, evaluating the Jahn-Teller and spin-orbit operators using the ${}^3_{s_z}E'_\pm$ states yields

$$H(s_z) = \frac{1}{2}K\rho^2 + \begin{pmatrix} -s_z\xi & -v_{e'}Q_+ \\ -v_{e'}Q_- & s_z\xi \end{pmatrix} \quad (5)$$

where $\xi = \langle {}^3_{+1}E_{x^2-y^2} | \hat{H}_{SO} | {}^3_{+1}E_{xy} \rangle$. Using Eq. 5 we observe that when the distortions are zero the spin-orbit coupling stabilizes the states according to the projection of their total angular

momentum as the orbital moment is unquenched. However, it is important to note that in TBP systems angular momentum is not conserved and should be taken as an effective quantity. Thus, Eq. 5 leads to three groups of two degenerate states (Fig. 3) where those with $|J_z| = |L_z + S_z| = 3$ (${}^3_{+1}E'_+$, ${}^3_{-1}E'_-$) are lowest, followed by those with $|J_z| = 2$ (${}^3_0E'_+$, ${}^3_0E'_-$) and $|J_z| = 1$ (${}^3_{+1}E'_-$, ${}^3_{-1}E'_+$). From this scheme, we see that the spin-reversal barrier at the high-symmetry configuration is simply ξ that coincides with Ni(II) spin-orbit coupling constant when covalency is fully neglected. While in systems with orbital degenerate states the usual spin-Hamiltonians are not valid²⁸ experimentally the value of ξ is usually assigned to the ZFS parameter, D.

However, when the system is allowed to distort, the JT terms in Eq. 5 become non-zero, mixing states with different values of the projection of the angular momentum, J_z , quenching the spin-orbit coupling. In a similar way, the states at the high-symmetry configuration with $s_z \neq 0$ are no longer orbitally degenerate (Eq. 5) and the JT is reduced due to Ham's effect and transformed into a pseudo JT effect³⁸. On the other hand for $s_z = 0$ states orbital degeneracy is retained and the JT effect keeps its full strength. As a consequence, when a distortion takes place the $s_z = 0$ states come closer to those with $s_z = \pm 1$ reducing the spin-reversal barrier and recovering the initial spin degeneracy corresponding with a triplet. Numerically this can be deduced from the solutions of Eq. 5:

$$E_{\pm}(s_z \neq 0) = \frac{1}{2}K\rho^2 \pm \sqrt{v_{E'}^2\rho^2 + \xi^2} \quad (6)$$

$$E_{\pm}(s_z = 0) = \frac{1}{2}K\rho^2 \pm v_{E'}\rho \quad (7)$$

In order to obtain a maximum value of the reversal barrier the distortion due to the JT effect must be fully destroyed. Expanding Eq. 6 to the second order in ρ we get:

$$E_{-} \approx -\xi + \frac{1}{2} \left(K - \frac{v_{E'}^2}{\xi} \right) \rho^2 + \dots \quad (8)$$

In Eq. 8 we observe that the energy is quadratic with the distortion and that the high-symmetry D_{3h} configuration is stable if $K > v_{E'}^2/\xi$ which is equivalent to $\xi > 2E_{JT}$ in the linear vibronic coupling approximation. If this condition is fulfilled the system will have a D_{3h} minimum and the value of the spin-reversal barrier will be equal to ξ which in D_{3h} Ni(II) complexes has a value close to the spin-orbit constant of the metal ion.

At this point it is important to note that the Hamiltonian given by Eq. 5 (essentially the same used in Refs.²⁹) does not connect the states with different s_z and, as a consequence, predicts magnetic tunneling to be zero, not allowing the decay of the total magnetization of a system. In order to produce a

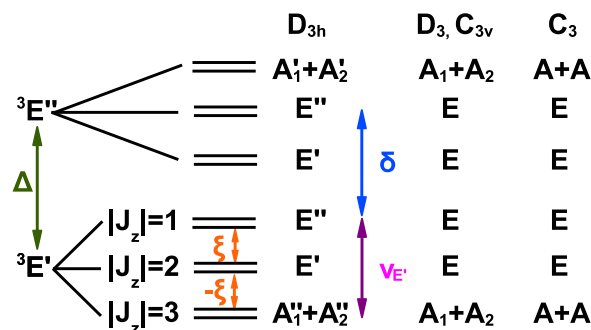


Fig. 3 (Color online) Diagram illustrating the splitting of the ground ${}^3E'$ state and the lowest excited ${}^3E''$ state due to the spin-orbit coupling. On the right-side of the figure we show the double group labels (in normal group notation, see text) for various initial structures of the TBP Ni(II) complex and the model's main parameters ($v_{E'}$, ξ , Δ and δ , see text).

realistic model for these phenomena it is necessary to include the coupling of ${}^3E'$ with excited states.

2.3 Magnetic tunneling

In order to proceed further, it is instructive to use double group symmetry. As the spin of Ni(II) is an integer, the use of double groups does not require to introduce irreps with new characters, allowing us to employ the labels of the normal point group, which facilitates following the coupling to vibrations and, at a later stage, understanding the effect of lowering the complex symmetry. In Fig. 3 we show the splitting of ${}^3E'$ state according to the double group labels. We see that the picture given in the previous section largely remains; the $|J_z| = 1, 2$ states remain degenerate by symmetry but the ground $|J_z| = 3$ state is separated into A_1'' and A_2'' . Our main objective, characterizing magnetic tunneling, is clearly related to this splitting. By similarity with the tunneling wavefunctions of a vibrational double well these states can be written as even and odd functions with respect to the magnetization:

$$|A_1''\rangle = \frac{1}{\sqrt{2}} (|{}^3_{+1}E'_+\rangle + |{}^3_{-1}E'_-\rangle) \quad (9)$$

$$|A_2''\rangle = \frac{1}{\sqrt{2}} (|{}^3_{+1}E'_+\rangle - |{}^3_{-1}E'_-\rangle) \quad (10)$$

However, using this transformation does not lead to any change in the energies obtained in the previous section as the splitting of these levels comes from interaction with excited terms. We consider here two kinds of interactions, one is direct, increasing the energy separation of A_1'' or A_2'' at the D_{3h} high-symmetry configuration and another via JT vibrations. It can be easily checked that none of the low-energy excited

states shown in Fig. 1 can be directly coupled to the two tunneling functions via spin-orbit interactions, thus, and as will be confirmed by *ab initio* calculations, the initial gap between these levels, that we will denote E_0 , is very small. On the other hand, these wavefunctions, are connected through e' vibrations to the $|J_z| = 1$ states. While in the previous section we found that this coupling does not produce a splitting in the ground state, consideration of the spin-orbit interaction with states coming from the ${}^3E''$ term (see Fig. 3) changes this situation. Using perturbation theory it can be shown (see Supporting information †) that the mixing of $|J_z| = 1$ states with the $s_z = 0$ components of ${}^3E''$ through spin-orbit interactions and JT distortions leads to a splitting, E , of A_1'' and A_2'' states equal to:

$$E \approx E_0 + \frac{\delta^2 v_{e'}^2}{\xi^2 (\Delta + \xi + v_{e'} \rho)} \rho^2 \quad (11)$$

where $v_{E''}$ is the JT constant of the ${}^3E''$ state, Δ is the energy of the lowest ${}^3E''$ term with respect to the ${}^3E'$ one and $\delta = \langle {}^3_{+1}E'_{x^2-y^2} | \hat{H}_{so} | {}^3_{0}E''_{xz} \rangle$ (see Fig. 3). Eq. 11 can be interpreted as the value of the *rhombohedral* magnetic anisotropy (E) with the distortion, ρ , close to the high-symmetry configuration. From the point of SIM design this geometry is the most interesting point of the energy landscape as the spin-reversal barrier is maximum and tunneling is minimum. Looking at Eq. 11 we see that E is not zero at D_{3h} , which is another indication that the usual spin Hamiltonians are not valid to describe orbitally degenerate states²⁸. Another contribution to tunneling at the high-symmetry geometry comes from the vibrational fluctuations existing even at T=0K (spin-phonon coupling). If the minimum occurs at the high-symmetry configuration vibrations have a force constant given by Eq. 8, $K_T = K - |v_{e'}|^2/\xi > 0$. To take into account the dispersion of the vibrational wavefunctions and calculate the spin-phonon contribution to tunneling we evaluate Eq. 11 with a bi-dimensional e' harmonic oscillator function of frequency $\omega = \sqrt{K_T/M}$ and average for temperature obtaining:

$$E(T) \approx E_0 + \frac{\delta^2 v_{e'}^2}{2\xi^2 (\Delta + \xi) \sqrt{K_T M}} (1 + 2\langle n(T) \rangle) \quad (12)$$

where $\langle n(T) \rangle$ is the average vibrational quantum at temperature T . Armed with this equation it is possible to discuss how to optimize the spin stability in Ni(II) TBP complexes by a careful choice of ligands.

The first thing we note is that for systems with a local D_{3h} symmetry δ/ξ is approximately constant and equal to 1/2 so this ratio cannot be used to modulate the value of tunneling. Of the remaining factors, we note that a selection of relatively strong ligands would increase all of $v_{E'}$, Δ and ξ . While these parameters compete to, respectively, increase

($v_{E'}$) and decrease (Δ , ξ) tunneling, our *ab initio* calculations indicate that $v_{E'}$ is the dominant one. Thus, weaker ligands should be selected to reduce tunneling, taking into account that smaller values of $v_{E'}$, due to enhanced metal-ligand covalency, will also favor that the minimum configuration displays high-symmetry. Finally, Eq. 12 shows that high K_T and M values favor localization of the vibrational wavefunction and a reduction of tunneling. Thus, SIM behavior for Ni(II) complexes should be expected only when using massive, bulky and/or rigid ligands that do not allow the system to distort. However, we should mention here a main caveat about using *massive* ligands. While they may be useful to achieve SIM behavior they also reduce the vibrational frequencies increasing the temperature-dependent term in Eq. 12. Thus, from the point of the blocking temperature only one solution seems feasible, the use of light and very rigid ligands that help to obtain SIM behavior and retain it to moderate temperatures.

While the theory above was developed for D_{3h} molecules, in practice many systems have lower symmetry. For instance, Ruamps et al.²⁹ report high-magnetic anisotropy in Ni(II) complexes that have an initial C_3 symmetry before taking into account any JT distortion. Symmetry has important consequences on this model as, for example, in some groups (D_{3h} , D_3) the spin-up and spin-down wavefunctions are equivalent and the tunneling functions given by Eqs. 9 and 10 are well-defined. In other groups (C_{3v} , C_3) the up and down directions are no longer equivalent and one of the spin-functions is lower in energy. This is particularly important in C_3 symmetry where both $|J_z| = 3$ functions have the same symmetry label (Fig. 3) and interact directly with one another. In this situation a relatively large tunneling gap is opened, favoring a quick magnetization decay. Reduction of symmetry also relaxes some of the symmetry constraints used in the construction of the model. However, *ab initio* calculations show that in cases where the local symmetry is close to D_{3h} , like in complexes (IV) and (V) below, these rules are still valid.

3 Computational details

The treatment of degeneracy and spin-orbit coupling in quantum mechanical systems is not straightforward and specially dedicated procedures are required.²⁷ In particular, no perturbational approaches like, i.e. Pederson-Khanna,⁴² can be used since the excitation energies are too small for these techniques to provide reliable results. In our case we use two methods of a different nature that allow us to cross-check our findings and that yield good agreement with available experimental data. The first is a modification of Density Functional Theory (DFT) to describe the multiplet levels in transition metal complexes, denominated ligand-field-DFT (LF-DFT) and developed by Daul et al.⁴³ which has been proved to be reasonably accurate for the calculation of magnetic properties^{44,45}. It allows ob-

taining the Racah's and ligand field parameters describing the excited states of a complex by calculating the energies of all the microstates of a d^n configuration by means of constrained DFT. We used an implementation of this method that relies on the Amsterdam Density Functional (ADF) program⁴⁶ and employed a high-quality triple- ζ with polarization basis set. Calculations with this method were carried out at B3LYP level. Use of other functionals, e.g. at LDA and GGA level, provides qualitatively the same results. Details about LF-DFT procedure, as well as tabulation of all the non-empirically determined parameters for herein studied systems, can be found in ESI †(Section S2, Table S1),

The second method we employed is multi-reference configuration interaction (MRCI) as implemented in the Molpro package⁴⁷. While usually complete-active-space-self-consistent-function (CASSCF) is considered a standard method to obtain magnetic properties in SIMs (see i.e. Ref.²⁷) it is well known that inclusion of dynamic correlation is required to predict with accuracy the position of excited states, a feature of importance in the theory shown above. For that reason it is usual to correct CASSCF energies with perturbation energy using either the CASPT2 or NEVPT2 approaches³¹. However, these approaches do not correct the usual overestimation of ionicity in CASSCF calculations when evaluating, for example, the spin-orbit constant. These problems can be overcome with the use of MRCI.

In our CASSCF calculations we obtain all singlet and triplet terms (see Fig. 1) that come out of Ni(II) d^8 configuration, by employing an active space containing the five orbitals with mainly Ni(3d) character and the 8 electrons that occupy them. Due to calculation size restrictions we cannot correlate all electrons using MRCI and we consider excitations only from Ni(3d) orbitals and the ligands' 2p (or 3p) ones. In order to represent the wavefunction we employed a large VTZ basis sets. Tests carried out with other basis sets are in good agreement with those shown below.

Geometry optimization of Ni(II) complexes was carried out at the B3LYP level to obtain the structure of the high-symmetry configuration (belonging to D_{3h} , D_3 or C_3 point groups), the minimum-energy structure characterizing each of the three equivalent JT minima and the transition-state separating them. Geometry optimizations carried out at LDA or GGA level lead to similar structures (Tables S3 and S4 in ESI †). Due to the very demanding nature of the MRCI method it was not possible to carry out optimization at this level so we performed single-point calculations at all the stationary points found with DFT and obtained the intrinsic distortion path (IDP) connecting these points⁴⁸.

In MRCI spin-orbit coupling was introduced by evaluating the full spin-orbit operator using the MRCI wavefunctions of states coming from the d^8 configuration and then diagonalizing the resulting matrix to find the final total energies. In

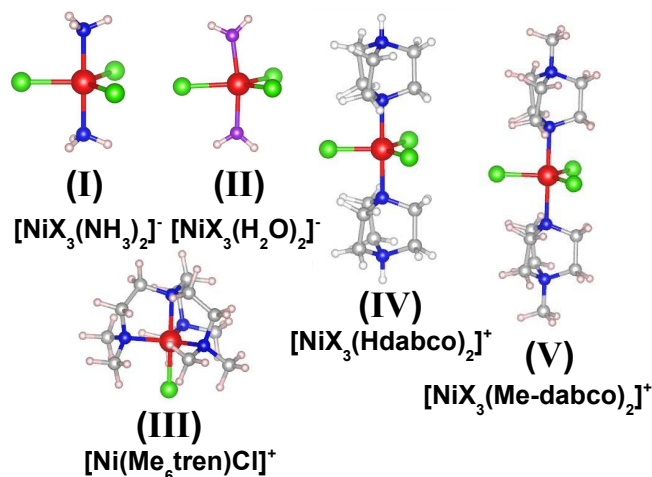


Fig. 4 (Color online) Scheme showing the complexes simulated in this work and the notation employed for them.

LF-DFT, spin-orbit coupling constant, used to obtain the spin-reversal barriers and the magnetic tunneling, was deduced from the least square fit of the energy splitting of the spinors, obtained by the relativistic Zero Order Regular Approximation (ZORA) spin-orbit DFT calculations, to the one-electron ligand field model (Table S1 in ESI †).

4 Results

In order to check the model presented in Section 2 we carried out calculations for several NiX_3Y_2 complexes, including some recently shown to display a strong magnetic anisotropy²⁹ (see Fig. 4). As the nature of the ground state of TBP Ni(II) systems is very sensitive to the nature of ligands, care must be taken in their choice to obtain a high-spin molecule. In order to probe the effect of equatorial ligand strength, we decided to use $X=F^-$ and Cl^- , because stronger ones, like CN^- or CO , lead to low-spin solutions. Similarly, axial ligands can be used to explore the effect of allowing the system to have the maximum D_{3h} symmetry with ligands like ammonia (I), or breaking it along a vertical plane using water (II), or an horizontal one like in $[Ni(Me_6tren)Cl]$ (Me_6tren is tris(2-dimethylaminoethyl)amine, III). Finally and with the objective of studying the effect of having bulky axial ligands over the interaction between the α and β angles (Fig. 2), we employed as axial ligands 1,4-diazabicyclo[2.2.2]-octane (dabco) (IV) as the structure^{35,36,49} and optical spectrum⁵⁰ of its Ni(II) complex with Cl^- equatorial ligands have been experimentally well characterized. Finally we checked the effect of long-range substitution in (IV) by replacing the terminal H in the cation $[NiX_3(Hdabco)_2]^+$ by methyl (Me) groups (V).

Table 1 Main results for the complexes studied in this work (see Fig. 4) for the high-symmetry and minimum configurations. The structure of the system is defined by its point group (PG), equatorial ($R(X_a), R(X_b)$) and axial ($R(Y)$) ligand distances. Values for complex (V) are not given as they are, essentially, the same as those of (IV). For full results please see Supporting information (Table S2 in ESI†). Distances are given in Å, angles in degrees and energies in cm^{-1} .

	System	PG	$R(X_a)$	$R(X_b)$	$R(Y)$	α	β	E_{JT}	D^{LF}	D^{MRCI}	E^{LF}	E^{MRCI}
(I)-F	[NiF ₃ (NH ₃) ₂] ⁻	D_{3h}	1.998	1.998	2.111	120.0	180.0	—	553	536	0.0	0.1
		C_{2v}	1.982	2.001	2.102	101.0	172.4	837	48	56	7.1	10.1
(I)-Cl	[NiCl ₃ (NH ₃) ₂] ⁻	D_{3h}	2.438	2.438	2.087	120.0	180.0	—	505	504	0.0	0.1
		C_{2v}	2.414	2.481	2.070	106.8	172.3	733	83	133	8.9	7.0
(II)-F	[NiF ₃ (H ₂ O) ₂] ⁻	C_{2v}	1.937	1.947	2.146	130.3	175.4	—	55	77	12.0	22.5
		C_{2v}	1.944	1.945	2.124	100.6	167.9	—	18	32	7.4	15.3
(II)-Cl	[NiCl ₃ (H ₂ O) ₂] ⁻	C_{2v}	2.371	2.365	2.134	126.2	178.5	—	205	183	2.4	8.1
		C_{2v}	2.350	2.382	2.114	105.7	167.7	—	41	67	9.8	10.6
(III)	[Ni(Me ₆ tren)Cl] ⁺	C_3	2.223	2.223	2.187/2.254	120.0	180.0	—	429	528	13.2	5.4
		C_1	2.154	2.244/2.275	2.168/2.268	113.5	176.3	711	146	116	8.0	2.3
(IV)-F	[NiF ₃ (Hdabco) ₂] ⁺	D_3	1.943	1.943	2.145	120.0	180.0	—	548	510	0.0	0.2
		C_2	1.932	1.943	2.148	112.1	179.2	726	128	132	0.7	1.8
(IV)-Cl	[NiCl ₃ (Hdabco) ₂] ⁺	D_3	2.337	2.337	2.281	120.0	180.0	—	498	524	0.0	0.2
		C_2	2.354	2.334	2.266	116.0	179.9	253	218	292	0.3	0.5

4.1 Comparison with experiment

The main results from our calculations are presented in Table 1 (see Supporting information for more details). Let us first establish their validity by comparison with available experimental data. Crystal X-ray diffraction experiments exist for complexes (III)²⁹, (IV)^{35,49} and (V)³⁶ with Cl⁻ ligands (denoted (IV)-Cl and (V)-Cl). For complex (III), our high-symmetry calculations show good agreement both in distances and angles with X-ray diffraction data. We have to mention here, that in this complex, Ruamps et al.²⁹ report the existence of a dynamic JT effect^{38,51,52} and predict the structure of the low-symmetry configuration using DFT calculations, and this result is also in agreement with ours. In the case of the dabco ligand [(IV)-Cl and (V)-Cl] we find that different works report slightly different structures. In some^{35,36} the equatorial triangle is slightly distorted ($\alpha \neq 120^\circ$) due to the low-symmetry packing of complexes inside the crystal. Using a different synthetic route Petrusenko et al.⁴⁹ could form chains with the complexes whose equatorial ligands show perfect equilateral triangle geometries. Our gas-phase results both for (IV) and (V) show a close agreement with experimental Ni-ligand distances, with errors of only 1-3pm. Before taking into account the spin-orbit coupling, DFT optimizations lead to an error of $\approx 4^\circ$ in the angle α that measures, to a large degree, the JT distortion of the complex. Experimentally this distortion is essentially non-existent⁴⁹ with small deviations only appearing due to packing forces in Refs.^{35,36}. However, when the spin-orbit coupling is taken into account (see below and the theory section) the JT effect existing in the ${}^3E'$ term is strongly quenched destroying the distortion in complexes (IV) and (V)

and leading to full agreement with experimental results.

Another important aspect that our calculations must capture is the ordering and spacing between the states. In order to test our methods we can compare the simulated transitions with the optical spectra of (IV-Cl) by Vallarino et al.⁵⁰ and of (III) by Ciampolini and Nardi.⁵³ In high-spin TBP Ni(II) complexes, experimentally the observed bands correspond to the transitions to the ${}^3E''$, ${}^3A'_2$, ${}^3E''$, ${}^3A'_2$ excited multiplets (in D_{3h} assignment). We find that the MRCI (LF-DFT) transitions in (IV)-Cl are at 4968 (5743), 13664 (8169), 18778 (14228), 20368 (15474) cm^{-1} which reasonably agree with the experimental values⁵⁰ of 5500, 10700, 17700, 20400 cm^{-1} . For the case of (III), MRCI (LF-DFT) transitions are 7275 (7139), 10667 (10675), 14655 (14036), 17503 (18236) and 21750 (19047) cm^{-1} , compared to the experimentally⁵³ observed 7100, 10900, 14900, 20600, 23500 cm^{-1} . We, thus see that our method provides reliable results both for structural properties and term position. More importantly, however, is how it performs with respect to the calculation of magnetic anisotropy. While multireference wavefunction *ab initio* methods like MRCI have already proved that they can provide semi-quantitative agreement with the experiment,^{19,26,27,29,31} LF-DFT has just shown its ability to predict the D values of some transition metal systems⁴³⁻⁴⁵. In Table 1 we see that LF-DFT and MRCI calculations lead to comparable results for all studied molecules providing both the same qualitative trends. Moreover, our estimated value of the axial ZFS for complex (III), 116-146 cm^{-1} , is in good consonance with both the theoretical (100-200 cm^{-1}) and experimental (120-180 cm^{-1}) D values reported in the recent work by Ruamps et al.²⁹. Additionally, while the LF-DFT is clearly overestimating the value

of the rhombic ZFS parameter, E , in (III), when compared to experiment ($E = 1.6 \text{ cm}^{-1}$), our MRCI calculations ($E = 2.3 \text{ cm}^{-1}$) come quite close to the EPR value. All this data show the adequacy of our simulations to understand the problem of anisotropy barriers and magnetic tunneling.

4.2 Structural effects of the ligands

Both the structural and magnetic properties of TBP-Ni(II) complexes are strongly dependent on the ligands. While both sets of properties are strongly correlated we will first discuss the effect of the ligands on the JT distortion and all magnetic properties will be studied in the next section.

Due to the somewhat restricted selection of ligands that yield a high-spin TBP Ni(II) complex we have obtained the equilibrium geometries of these systems for equatorial F^- and Cl^- ions. In Table 1 we see that the substitution $\text{F}^- \rightarrow \text{Cl}^-$ always brings a significant reduction of the JT distortion, as measured by the angle α and the JT energy. This decrease is particularly dramatic in $[\text{NiX}_3(\text{Hdabco})_2]^+$ where the JT energy goes from 726 cm^{-1} to 253 cm^{-1} upon the change in equatorial coordination. We find two main causes for this behavior: (a) the reduction in linear vibronic constant ($\nu_{E'}$) as covalency increases in Ni–Cl bonds when compared to the Ni–F ones and (b) the increase of the force-constant associated to the larger size of chlorine ions, leading to stronger in-plane ligand-ligand repulsions due to the bending nature of the mode. Since high-magnetic anisotropy and SIM behavior require small distortions, it seems clear that large equatorial ligands are a requirement to obtain these properties in Ni(II) complexes. Test calculations employing Br^- ions as equatorial ligands indicate that a small extra reduction in the distortion can be achieved using these larger ions.

Let us now explore the effect of axial ligands. The choice of these ligands can strongly alter the symmetry of the system, as for example, in complexes (I), (IV) and (V) the ammonia, Me_6tren , Hdabco and Me–dabco ligands allow, in first instance, retaining a third-order axis while H_2O -containing (II) does not. As a consequence, we see in Table 1 that complexes (II) are the ones yielding the highest bending angles, α and β , with the consequence that the spin-reversal barrier is the lowest for these systems. In fact, the correlation between large α and β angles is seen over all the molecules shown in Table 1. Obviously when water is used as a ligand the intrinsic reduction of symmetry helps distorting the equatorial ligand triangle. However, in all other cases axial ligand size seems to be crucial to explain this effect. This can be observed comparing complex (I) with complexes (IV) and (V). While in the first case the small size of ammonia allows it to introduce itself closer to the equatorial ligands, increasing β and as a consequence α , the bulky dabco ligands of (IV) and (V) simply cannot fit and β is very close to 180° . Since the axial ligands

do not favor the equatorial distortion we find that the latter is strongly diminished both in (IV) and (V) when compared to (I). Thus, a main requirement for potential SIM molecules in TBP Ni(II) complexes is that axial ligands must be as large as possible. Another possible strategy to restrict the equatorial ligand's movement is the use of tetradentate ligands like the one employed in complex (III) where we observe that the distortion ($\alpha = 113.5^\circ$) is sensibly smaller than, for example, the one in complex (I). However, and as we will see in the next section the initial C_3 symmetry in this complex and the significant off-center movement of the Ni(II) ion with respect to the equatorial N_3 plane leads to weakened magnetic properties.

4.3 Magnetic properties

In this section we are mainly interested in discussing the two ZFS parameters obtained from the calculation, D and E due to their relationship, respectively, with the spin-reversal barrier and tunneling splitting. Observing the values of $|D|$ in Table 1 we find that the maximum value is always obtained for the high-symmetry configuration and how Jahn-Teller distortions quickly reduce its value. In particular, we see that the larger the value of α at the minimum, the smaller the value of $|D|$ which makes complexes with small ligands (like F^- or ammonia) or ligands that break the symmetry (like water) to lose much of their interest as candidates to become SIMs. On the other hand complexes with large ligands like (III), (IV) or (V) present smaller distortions and their magnetic anisotropy is large, even in the distorted state. Thus, in order to achieve the maximum possible spin-reversal barrier the distortion has to be fully destroyed by the spin orbit coupling which, according to Eq. 8, only happens when $2E_{JT} < \xi$. Since ξ coincides with $|D|$ at the high-symmetry configuration, from the values in Table 1 we see that only complexes (IV)-Cl and (V)-Cl can fulfil this condition. In order to quantify this statement we have plotted in Fig. 5 the MRCI energy surface connecting the high-symmetry configuration with the global minimum and the Jahn-Teller transition state for $[\text{NiCl}_3(\text{Hdabco})_2]^+$ and $[\text{NiF}_3(\text{NH}_3)_2]^-$ when the spin-orbit coupling is taken into account. We see that while the minimum corresponds with a distorted configuration in the second case, in the first it occurs for $\alpha = 120^\circ$, in agreement with experimental results⁴⁹. Thus, at difference with complex (III) where Ruamps et al.²⁹ showed that the crystal third-order axis appeared due to the dynamic nature of the JT distortion, in (IV)-Cl calculations predict that the minimum energy structure is, indeed, the high-symmetry one. Thus, the maximum value of the spin-reversal barrier, U , is achieved for complexes (IV) and (V) with equatorial chloride ligands reaching a value close to 500 cm^{-1} , which is the largest one reported for a transition metal, including the recent record⁵⁴ found in linear Fe^+ complexes, $U = 226 \text{ cm}^{-1}$.

However, SIMs are not just characterized by a high mag-

netic anisotropy measured by, D , but also display *bistability* which can be achieved only when the tunneling splitting is small enough. In Table 1 we show the static part of tunneling, which can be associated to the experimental rhombic ZFS parameter, E , both for the high-symmetry configuration and the minimum and this variation can give an estimation of the spin-phonon coupling. According to Eq. 11 minimization of this quantity requires high Δ and ξ values and small vibronic constants $v_{E'}$ and $v_{E''}$. While larger Δ values are favored with stronger ligands this effect is compensated by the magnification of the linear vibronic constants and may lead, in the case of very strong ligands, to low-spin complexes that destroy magnetism. Thus, the best way to minimize the tunneling transition probability is by reducing the distortion to a minimum and increasing the force constant along the JT vibration modes as much as possible. This conclusion is supported by the results in Table 1: E is larger in complexes containing F^- when compared to those with Cl^- as they present more significant distortions. This can also be appreciated in Fig. 6, where the change of E along the distortion is shown for $[NiCl_3(Hdabco)_2]^+$ and $[NiF_3(NH_3)_2]^-$. We find that, in agreement with the perturbational model (Eq. 11), the increase of E around the high-symmetry configuration is quadratic and, numerically, the model performs well over this range until the closeness to one of the quickly descending $s_z = 0$ states (see in Fig. 5) produces a quick change in tendency. Moreover, even for small distortion the reduced vibronic coupling constant of complex (IV) makes the increase in E slower than that in (I). Thus, we see that control of the geometry is the key to achieve small tunneling values and that can be implemented using either bulky ligands like in complexes (IV) and

(V) or employing hard multidentate ligands like in (III). However, it is important to note that in these systems the value of E at the high-symmetry configuration is small but non-zero at difference of what one would expect when employing the usual spin-Hamiltonian for an axial system (Eq. 1), or LF theory (see Table 1) due to a lack of a detailed description of the influence of the ligands on the metal orbitals. In systems where the high-symmetry configuration is D_{3h} (like (I)) or where the symmetry of the metal and first-neighbors is D_{3h} (like (IV) and (V)) the initial tunneling splitting is very small ($E_0 \approx 0.1 - 0.2\text{cm}^{-1}$). On the other hand this value in (III) is much larger ($E_0 \approx 5\text{cm}^{-1}$) as in C_3 symmetry the two tunneling functions belong to the same irrep (Fig. 3) and their direct interaction opens a gap between them. Thus, we find that small tunneling values require both small distortions and an initial symmetry which is close to D_{3h} . These results support that $[NiCl_3(Hdabco)_2]^+$ and its variants are very interesting candidates for SIM behavior. On one hand the Jahn-Teller distortion is fully quenched giving rise to a very high magnetic anisotropy, $D \approx 500\text{cm}^{-1}$ which, to our knowledge, is the largest predicted for a transition-metal complex. Furthermore, comparison of the tunneling of this system at the minimum-energy position (when including the effect of spin-orbit coupling) shows that it is an order of magnitude smaller ($E = 0.2\text{cm}^{-1}$) than in any other complex contained in Table 1. Thus, our calculations predict that magnetic states in complexes (IV)-Cl or (V)-Cl are much more stable than in (I) or (III). However, the tunneling frequency characterizing the timescale in which a spin can be observed as stable by magnetic measurements is still too high (of the order of 1GHz) to yield SIM behavior. On the other hand, and due to the substantial reduction of tunneling splitting in these systems, the magnetic dynamics in these complexes can be strongly perturbed by external magnetic fields^{15,25} of reasonable intensity ($\approx 0.1T$). As a consequence, these molecules are excellent candidates to find slow magnetic relaxation in a Ni(II) complex for the first time, albeit under a constant magnetic field.

Finally, we would like to remark that the strong coupling of geometry and magnetic anisotropy can also be used to externally manipulate the spin. In TBP systems like $[NiCl_3(Hdabco)_2]^+$ a JT distortion induces an in-plane electric dipole that can couple with electric fields in this direction. Thus, application of an electric field will strongly favor JT-type distortions that have a very low-frequency (as shown in Fig. 5) that could be used to enhance the tunneling rate allowing to alter the spin orientation in devices.

5 Conclusions

In this work we have shown that controlling the geometry of a transition metal complex presenting an orbital degenerate state can lead to a complete destruction of the Jahn-Teller

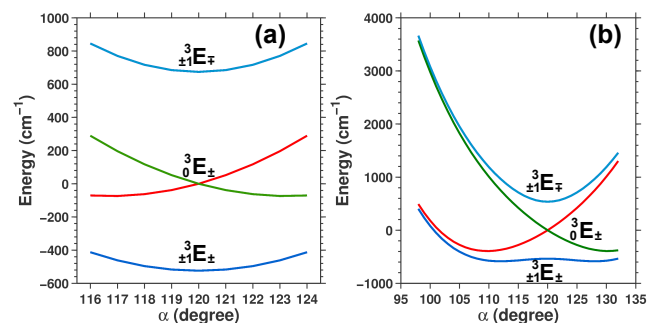


Fig. 5 (Color online) Energy surface cross-section calculated at the MRCI level along the intrinsic distortion path⁴⁸ going from the D_3 ($[NiCl_3(Hdabco)_2]^+$), (a) / D_{3h} ($[NiF_3(NH_3)_2]^-$), (b) high-symmetry configuration to the C_{2v}/C_2 minima and transition states. The doubly degenerate $|M_s| = 1$ states are shown by dashed blue lines while the $M_s = 0$ ones are represented with solid red and green lines.

distortion by the spin-orbit coupling. The main consequence of this fact is that the system will display a very large magnetic anisotropy creating a high barrier between the two states with largest spin projection, a fundamental step in the rational design of single-ion magnets. Moreover, and for the first time, we give an expression containing the main chemical ingredients participating in the magnetic tunneling that controls whether a particular system displays SIM behavior and its blocking temperature. As a salient feature these models show that higher blocking temperatures could be achieved with very rigid but light ligands. These models have been corroborated by using state-of-the-art computational methods, showing that the $[\text{NiCl}_3(\text{Hdabco})_2]^+$ cation has a value of $D = -524 \text{ cm}^{-1}$ which is large enough to prevent the thermal transition between the states on both sides of the barrier even at room temperature and a tunneling splitting rate which is, at least, an order of magnitude smaller than similar molecules with a high-magnetic anisotropy and is, as a consequence, an excellent candidate to be the first Ni(II) SIM. Furthermore, the fact that geometry, dipole moment and magnetic anisotropy are strongly connected allows to design methods to manipulate the barrier using external means like mechanical or electric perturbations opening new venues of research in the properties of these interesting complexes.

6 Acknowledgments

This project was supported by the Serbian-Spanish collaboration project Number PRI-AIBSE-2011-1230 and 451-03-02635/2011-14/5, the Spanish Ministerio de Industria e Innovación under project FIS2009-07083 and the Serbian Ministry of Science under project 172035. The COST-CMTS Action CM1002 “Convergent Distributed Environment for Computational Spectroscopy (CODECS)” is also acknowledged. We would like to thank Profs. M. Moreno and J.A. Aramburu for

reviewing the manuscript and to Prof. C. Daul for various discussions concerning LF-DFT method.

References

- R. Sessoli, D. Gatteschi, A. Caneschi and M. A. Novak, *Nature*, 1993, **365**, 141–143.
- M. Mannini, F. Pineider, P. Saintavitt, C. Danieli, E. Otero, C. Sciancalepore, A. M. Talarico, M.-A. Arrio, A. Cornia, D. Gatteschi and R. Sessoli, *Nat. Mat.*, 2009, **8**, 194–197.
- P. C. E. Stamp and A. Gaita-Arino, *J. Mat. Chem.*, 2009, **19**, 1718–1730.
- L. Bogani and W. Wernsdorfer, *Nat. Mat.*, 2008, **7**, 179–186.
- A. Hauser, C. Enachescu, M. L. Daku, A. Vargas and N. Amstutz, *Coord. Chem. Rev.*, 2006, **250**, 1642–1652.
- P. Garcia-Fernandez and I. B. Bersuker, *Phys. Rev. Lett.*, 2011, **108**, 246406.
- D. Gatteschi, R. Sessoli and J. Villain, *Molecular Nanomagnets*, Oxford University Press, 2006.
- J. R. Friedman, M. P. Sarachik, J. Tejada and R. Ziolo, *Phys. Rev. Lett.*, 1996, **76**, 3830–3833.
- C. Sangreforio, T. Ohm, C. Paulsen, R. Sessoli and D. Gatteschi, *Phys. Rev. Lett.*, 1997, **78**, 4645–4648.
- K. Katoh, Y. Horii, N. Yasuda, W. Wernsdorfer, K. Toriumi, B. Breedlove and M. Yamashita, *Dalton Trans.*, 2012, **41**, 13582–13601.
- L. Vitali, S. Fabris, A. M. Conte, S. Brink, M. Ruben, S. Baroni and K. Kern, *Nano Lett.*, 2008, **8**, 3364–3369.
- C. J. Milios, A. Vinslava, W. Wernsdorfer, S. Moggach, S. Parsons, S. P. Perlepes, G. Christou and E. K. Brechin, *J. Am. Chem. Soc.*, 2007, **129**, 2754–2755.
- S. D. Jiang, B. W. Wang, H. L. Sun, Z. M. Wang and S. Gao, *J. Am. Chem. Soc.*, 2011, **133**, 4730–4733.
- J.-N. Rebilly, G. Charron, E. Rivière, R. Guillot, A.-L. Barra, J. D. Serano, J. van Slageren and T. Mallah, *Chem. Eur. J.*, 2008, **14**, 1169–1177.
- W. H. Harman, T. D. Harris, D. E. Freedman, H. Fong, A. Chang, J. D. Rinehart, A. Ozarowski, M. T. Sougrati, F. Grandjean, G. J. Long, J. R. Long and C. J. Chang, *J. Am. Chem. Soc.*, 2010, **132**, 18115–18126.
- J. M. Zadrozny and J. R. Long, *J. Am. Chem. Soc.*, 2011, **133**, 20732–20734.
- O. Waldmann, *Inorg. Chem.*, 2007, **46**, 10035–10037.
- F. Neese and D. A. Pantazis, *Far. Discuss.*, 2011, **148**, 229–238.
- E. Ruiz, J. Cirera, S. Alvarez, C. Loose and J. Kortus, *Chem. Comm.*, 2008, 52–54.
- A. Trueba, P. Garcia-Fernandez, F. Senn, C. A. Daul, J. A. Aramburu, M. T. Barriuso and M. Moreno, *Phys. Rev. B*, 2010, **81**, 075107.
- N. Ishikawa, M. Sugita, T. Ishikawa, S. Koshihara and Y. J. Kaizu, *J. Am. Chem. Soc.*, 2003, **125**, 8694–8695.
- R. Sessoli and A. K. Powell, *Coord. Chem. Rev.*, 2009, **253**, 2328–2341.
- G.-J. Chen, Y.-N. Guo, J.-L. Tian, J. Tang, W. Gu, X. Liu, S.-P. Yan, P. Cheng and D.-Z. Liao, *Chem. Eur. J.*, 2012, **18**, 2484–2487.
- J. D. Rinehart and J. R. Long, *Chem. Sci.*, 2011, **2**, 2078–2085.
- D. E. Freedman, W. H. Harman, T. D. Harris, G. J. Long, C. J. Chang and J. R. Long, *J. Am. Chem. Soc.*, 2010, **132**, 1224–1225.
- J. Cirera, E. Ruiz, S. Alvarez, F. Neese and J. Kortus, *Chem. Eur. J.*, 2009, **15**, 4078–4087.
- M. Atanasov, D. Ganyushin, D. A. Pantazis, K. Sivalingam and F. Neese, *Inorg. Chem.*, 2011, **50**, 7460–4477.
- A. Pali, J. M. Clemente-Juan, E. Coronado, S. Klokishner, S. M. Ostrovsky and O. S. Reu, *Inorg. Chem.*, 2010, **49**, 8073–8077.
- R. Ruamps, R. Maurice, L. Batchelor, M. Boggio-Pasque, P. Guillot, A. Barra, J. Liu, E. Bendeif, S. Pillet, S. Hill, T. Mallah and N. Guihery, *J. Am. Chem. Soc.*, 2013, **135**, 3017–3026.

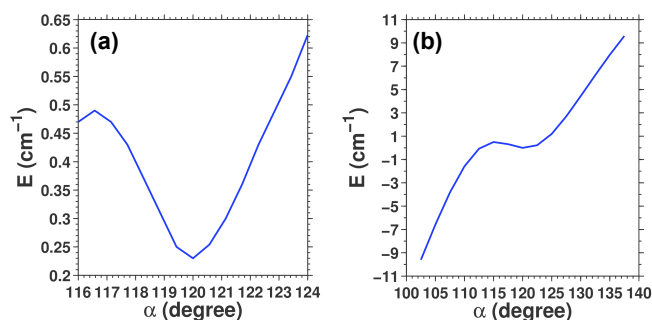


Fig. 6 (Color online) Magnetic tunneling splitting along the intrinsic distortion path⁴⁸ as calculated for $[\text{NiCl}_3(\text{Hdabco})_2]^+$, (a) and $[\text{NiF}_3(\text{NH}_3)_2]^-$ (b).

- 30 J. M. Zadrozny, M. Atanasov, A. M. Bryan, C.-Y. Lin, B. D. Rekker, P. P. Power, F. Neese and J. R. Long, *Chem. Sci.*, 2013, **4**, 125–138.
- 31 M. Atanasov, J. M. Zadrozny, J. R. Long and F. Neese, *Chem. Sci.*, 2013, **4**, 139–156.
- 32 S. Gomez-Coca, E. Cremades, N. Aliaga-Alcalde and E. Ruiz, *J. Am. Chem. Soc.*, 2013, **135**, 7010–7018.
- 33 J. Bendix, M. Brorson and C. E. Schäffer, *Inorg. Chem.*, 1993, **32**, 2838–2849.
- 34 D. Gatteschi and R. Sessoli, *Angew. Chem. Int. Ed.*, 2003, **42**, 268–297.
- 35 R. G. Pritchard, M. Ali, A. Munim and A. Uddin, *Acta Cryst.*, 2006, **C62**, 507–509.
- 36 W. J. Rozell and J. S. Wood, *Inorg. Chem.*, 1977, **16**, 1827–1833.
- 37 S. M. W. Domcke and L. Poluyanov, *Chem. Phys.*, 2006, **322**, 405–410.
- 38 I. B. Bersuker, *The Jahn-Teller Effect*, Cambridge University Press, 2006.
- 39 R. S. Berry, *J. Chem. Phys.*, 1960, **32**, 933–938.
- 40 P. Garcia-Fernandez, I. Bersuker, J. Aramburu, M. Barriuso and M. Moreno, *Phys. Rev. B*, 2005, **71**, 184117.
- 41 H. Longuet-Higgins, *Proc. Roy. Soc. London*, 1975, **A351**, 147.
- 42 M. R. Pederson and S. N. Khann, *Phys. Rev. B*, 1999, **60**, 9566–9572.
- 43 M. A. Atanasov, C. A. Daul and C. Rauzy, *Chem. Phys. Lett.*, 2003, **367**, 737–746.
- 44 M. Atanasov and C. Daul, *C. R. Chimie*, 2005, **8**, 1421–1434.
- 45 M. Atanasov, C. Rauzy, P. Baettig and C. Daul, *Int. J. Quan. Chem.*, 2005, **102**, 119–131.
- 46 G. te Velde, F. M. Bickelhaupt, S. J. van Gisbergen, C. F. Guerra, E. J. Baerends, J. G. Snijders and T. J. Ziegler, *Comput. Chem.*, 2001, **22**, 931–967.
- 47 H.-J. Werner, P. J. Knowles, G. Knizia, F. R. Manby, M. Schütz, P. Celani, T. Korona, R. Lindh, A. Mitrushenkov, G. Rauhut, K. R. Shamasundar, T. B. Adler, R. D. Amos, A. Bernhardsson, A. Berning, D. L. Cooper, M. J. O. Deegan, A. J. Dobbyn, F. Eckert, E. Goll, C. Hampel, A. Hesselmann, G. Hetzer, T. Hrenar, G. Jansen, C. Köppl, Y. Liu, A. W. Lloyd, R. A. Mata, A. J. May, S. J. McNicholas, W. Meyer, M. E. Mura, A. Nicklass, D. P. O'Neill, P. Palmieri, D. Peng, K. Pflüger, R. Pitzer, M. Reiher, T. Shiozaki, H. Stoll, A. J. Stone, R. Tarroni, T. Thorsteinsson and M. Wang, *MOLPRO, version 2012.1, a package of ab initio programs*, 2012, see <http://www.molpro.net>.
- 48 M. Gruden-Pavlović, P. Garcia-Fernandez, L. Andjelković, C. Daul and M. Zlatar, *J. Phys. Chem. A*, 2011, **115**, 10801–10813.
- 49 S. R. Petrusenko, J. Sieler and V. Kokozay, *Zeit. für Natur.*, 1997, **300**, 331–336.
- 50 L. Vallarino, V. Goedken and J. Quagliano, *Inorg. Chem.*, 1972, **11**, 1466–1469.
- 51 P. Garcia-Fernandez, A. Trueba, M. Barriuso, J. Aramburu and M. Moreno, *Phys. Rev. Lett.*, 2010, **104**, 035901.
- 52 P. Garcia-Fernandez, A. Trueba, M. Barriuso, J. Aramburu and M. Moreno, in *Vibronic Interactions and the Jahn-Teller Effect*, ed. M. Atanasov, C. Daul and P. L. Tregenna-Piggott, Springer Netherlands, 2012, vol. 23, pp. 105–142.
- 53 M. Ciampolini and N. Nard, *Inorg. Chem.*, 1966, **5**, 41–44.
- 54 J. M. Zadrozny, D. J. Xiao, M. Atanasov, G. J. Long, F. Grandjean, F. Neese and J. R. Long, *Nat. Chem.*, 2013, **5**, 577–581.